Determination of optical constants from Martian analog materials using a spectro-polarimetric technique

G. Alemanno, E. Garcia-Caurel, J. Carter, François Poulet, R. Brunetto, Alice Aléon-Toppani, R.G. Urso, O. Mivumbi, Claire Boukari, Vincent Godard, et al.

Version of Record: https://www.sciencedirect.com/science/article/pii/S0032063320303512
Manuscript_b9bc3de06e0fa5f034cf2fcaf456fcf6

Determination of optical constants from Martian analog materials using a spectro-polarimetric technique

G. Alemanno[1,*], E. Garcia-Caurel[2], J. Carter[1], F. Poulet[1], R. Brunetto[1], A. Alèon-Toppani[1], R. G. Urso[1], O. Mivumbi[1], C. Boukari[3], V. Godard[3], Borondics F.[4]

[1]Universitè Paris-Saclay, CNRS, Institut d'astrophysique spatiale, 91405, Orsay, France

[2]LPICM, CNRS, Ecole Polytechnique, IPParis, 91128 Palaiseau, France

[3]CNRS GEOPS UMR 8148 Bassin et Ressources, Bâtiment 504, Orsay, Cedex, France

[4]Synchrotron Soleil, L'Orme des Merisiers, Saint-Aubin–BP48, 91192 Gif-sur-Yvette CEDEX, France

Abstract

The technique of spectroscopic ellipsometry is a powerful tool for the characterization of the optical properties of materials. This technique represents a significant refinement over the semi-empirical approach to optical constants determination using BRDF (Bidirectional Reflectance Distribution Function) measurements of a finite set of grain sizes for each mineral. It also allows obtaining, not only the optical constants, but also information about the dependence of optical response on sample orientation respect to the illuminating light beam. In this work, we present our experimental approach to derive optical constants of Martian analogue materials based on an infrared ellipsometry technique. We derived the optical constants of gypsum between 750 and 5000 cm^{-1} (2 – 13 μm) using data obtained with an infrared spectroscopic Mueller ellipsometer. Thanks to the high sensitivity of the ellipsometric measurements, and despite of a rather complex data analysis protocol, the results obtained for the gypsum samples show that it is possible to successfully use this technique for direct determination of optical constants of natural minerals. The method discussed here can provide the planetary science community with laboratory derived optical constants of a large number of minerals and materials (either natural or synthetic).

*_Current address:_ German Aerospace Center (DLR), Rutherfordstrasse 2, D-12489 Berlin, Germany (giulia.alemanno@dlr.de)

1. Introduction

One of the most outstanding scientific issues of our time is to understand if life ever emerged on Mars and whether its record could have been preserved over geologic eons. The planet presents evidence that liquid water was abundant at the surface early in its history (e.g. Alemanno et al., 2018; Orofino et al., 2018; and references therein), which in turn may have spawned habitable environments. In particular, orbital spectroscopic data have shown the widespread presence of aqueous alteration minerals on the Martian surface, including hydrous clays composed by phyllosilicates and hydrated salts (e.g. Ehlmann and Edwards, 2014; Carter et al., 2013; Bibring et al., 2006). Several hypotheses have been advanced to explain the possible formation mechanisms of these mineral assemblages, which yield very different implications for the paleoclimate of the planet and its exobiological emergence/preservation potential. To both better constrain early Mars conditions and to deal with the increasing quantity of data available, more and more detailed analysis and effort for their interpretation are required. Several spectrometers are currently in orbit around Mars, including the Thermal Emission Spectrometer (TES) onboard Mars Global Surveyor (Christensen et al., 2001), the imaging spectrometer Observatoire pour la Mineralogie, l'Eau, le Glace e l'Activité (OMEGA) (Bibring et al., 2006) the Planetary Fourier Spectrometer (PFS) (Formisano et al., 2005) onboard Mars Express; the Compact Reconnaissance Imaging Spectrometer for Mars (CRISM) onboard Mars Reconnaissance Orbiter (Murchie et al., 2007); the NOMAD spectrometer (Nadir and Occultation for MArs Discovery) (Vandaele et al., 2015) and the Atmospheric Chemistry Suite (ACS) of spectrometers (Korablev et al. 2018) onboard of ExoMars2016 mission. Terabytes of data collected from these instruments are currently available. However, the correct interpretation of these data requires the complicated problem of isolating each of the atmospheric and surface components and determining their relative contribution to the measured radiance signal. In this context, the knowledge of optical constants is a key for the detectability and understanding of the distribution, abundance, and type of minerals on Mars using remote-sensing spectral data.

Optical constants describe the interaction of matter with an electromagnetic radiation, taking into account the vibrational and electronic transitions for each wavelength. Particulate matter exists in the Earth's atmosphere and surface as well as in the atmospheres and on the surfaces of other planetary bodies and in circumstellar clouds. This matter scatters and absorbs both sunlight and superficial thermal radiation. The values of the optical constants are therefore fundamental to characterize planetary surfaces and atmospheres and correctly describe a variety of physical environments like planetary atmospheres, circumstellar clouds, material abundances on a planet's surfaces and the behavior of satellites' regolith (Marzo et al., 2004).

Applied to remote sensing data of planetary surfaces, optical constants enable making quantitative estimates of the mineralogical composition (e.g. Poulet et al., 2008). However, to interpret the spectra acquired from the surface of a planetary body, an appropriate radiative transfer model is necessary to take into account the combined influence of the atmospheric aerosol and gas, and the surface (e.g. Shkuratov et al., 1999; Poulet and Erard, 2004; Poulet et al., 2008). Radiative transfer models describe the interaction between surface and atmosphere and allow for a proper determination of the effect of these particles on the optical measurements acquired from the surface of a planet. However, to do this, such models require a good knowledge of the optical constants for each component that may be present on the area under examination (Poulet et al., 2002; Poulet et al., 2014). Applying these models is difficult in the NIR and MIR due to the lack of reliable optical constants for many important minerals in the monoclinic and triclinic crystal systems.

In particular, in the case of Mars, thanks to high-resolution mapping using visible and near infrared spectrometers in orbit around the planet, it has been possible to reveal the presence of several and diverse mineral deposits on the Martian surface (Poulet et al., 2005; Bibring et al.; 2006, Carter et al., 2013). However, quantitative analysis within these deposits can provide important knowledge on the type of process that forms them (e.g. allowing to distinguish between depositional and diagenetic mechanism). This information will be essential to better understand the nature of global and local-scale variations in the presence and proportions of different type of minerals on the planet's surface (Stack and Milliken, 2015).

In this work we discuss a method to obtain the optical constants of Martian analogue materials in the mid-far infrared range using spectroscopic Mueller ellipsometry technique, which is an extension of standard ellipsometry. Ellipsometry consists of the use of polarized light to characterize the optical properties of materials, either in bulk or in thin film format. In standard ellipsometry the light beam must remain completely polarized during the whole measurement process (Garcia-Caurel et al., 2015). However, Mueller ellipsometry, being a generalization of standard ellipsometry, allows to properly measure and interpret the properties of partially polarized light (Garcia-Caurel et al., 2015). Therefore, this method can be used to measure inhomogeneous and/or anisotropic samples if an appropriate model, which accounts for such non-homogeneity, is used to interpret experimental data. In the infrared range, the dielectric function is sensitive to vibrational absorptions related to molecular bonds. Therefore, infrared ellipsometry can be used to study chemical composition, crystallinity or doping levels of different types of materials, such as semiconductors, oxides or polymers (Garcia-Caurel et al., 2015).

Despite being widely used to characterize the optical constants of thin films, spectroscopic ellipsometry has been scarcely used to determine the optical constants of planetary analog materials

or similar minerals. The purpose of this study is to implement this technique for the determination of the optical constants of materials of Martian interest such as hydrated silicates (such as phyllosilicates, hydrated silica) and evaporites (such as carbonates, sulfates and chlorides) with the main goal of providing the scientific community with missing data on optical constants on these kinds of materials.

Here, we present the developed measurement protocol and the data modelling procedure that has the potential to be extended and applied to the study of large variety of materials and planetary surfaces. For the sake of illustration, in this work, the use of ellipsometry has been applied on a set of gypsum samples (Section 2.1). In the following sections, we present the experimental methodology, including sample choice and preparation protocol, experimental setup and procedure (Section 2), the data modeling (Section 3). The results obtained for the gypsum samples are shown in Section 4. Discussions on the results obtained along with comparisons with literature are reported in Section 5. Finally, Section 6 discusses the overall methodology and future developments. In addition, more details about the data modeling procedure are described in Appendix A together with the presentation of some cases of study.

2. Experimental methodology

2.1 Sample preparation protocol

Gypsum ($CaSO4 \cdot 2H2O$), a hydrated calcium sulfate characterized by a monoclinic crystal structure, is a very common mineral on Earth. We decided to focus our study on gypsum samples for three main reasons: 1) its common identification on Mars; 2) its availability in samples sizes that are suitable for studies that imply different types of spectral measurements; 3) several studies report the optical constants of gypsum in the mid-infrared (Aronson et al., 1983; Long et al., 1993; Marzo et al., 2004, Roush et al., 2007) that can be used as comparison to evaluate our approach.

The presence of sulfate on the Martian surface could be a strong indication of the past presence of liquid water on Mars (e.g. Marzo *et al*., 2006). This may have, in turn, important astrobiological implications. Gypsum and sulfate salts in general have also been identified by space agencies as a key resource for future exploration (ISRU, InSitu Ressource Utilization). Gypsum would provide, in addition to building material, a source of extractable water.

Samples of a superficial gypsum from acid-sulfate alteration in the Myvatn geothermal area in Iceland, have been used as target of our study. Preliminary FTIR spectra acquired in the visible near infrared (VISNIR) between 4000 and 10000 cm^{-1} (1-2.6 µm) showed no obvious contaminants in the samples integrated over the ~3 mm beam in hemispheric reflectance (see Fig. 1).

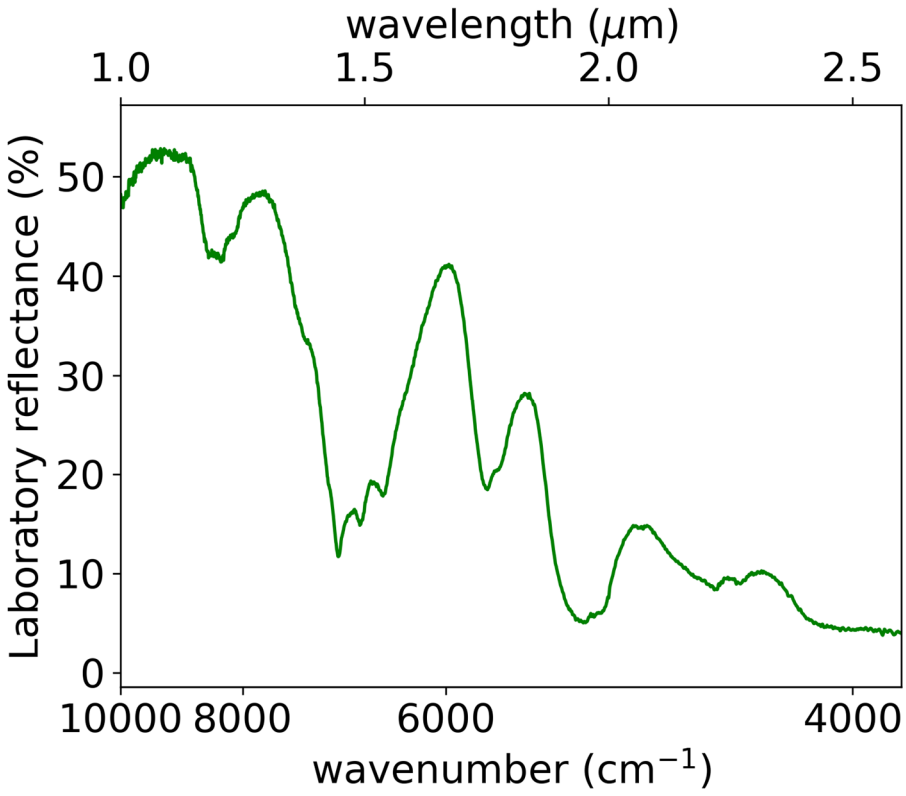

Fig. 1 – Example of a VISNIR spectrum acquired on our gypsum sample between 4000 and 10000 cm^{-1} (1-2.6 µm).

In gypsum, the crystallographic axes are defined by the following parameters: a = 5.679(5) Å, b = 15.202(14) Å, c = 6.522(6) Å, β = 118.43(4)°, and Z = 4 according to Pedersen, 1982. The ideal chemical formula of gypsum is $CaSO_4 \cdot 2H_2O$ and the crystal has a stratified structure, with the layers lying along the crystallographic plane (010). Two layers of sulfate ions are bound together by calcium to form a robust double sheet. The double layers are linked together by sheets of water molecules. Each calcium ion is eight coordinated, six of these links are to oxygen atoms belonging to sulfate atoms, and the remaining two links are to two oxygen atoms belonging to water molecules. The monoclinic plane in gypsum intercepts axes a, and c, while the axis b is mutually perpendicular to a, and c. The unit cell of gypsum includes different phosphate tetrahedra which are oriented along different directions in space. In the measurements performed in this work samples were cut and polished along the facile cleavage faces which are parallel to the crystallographic plane (010) (Pedersen, 1982, Antony, 1990), therefore the b axis was perpendicularly oriented to the surface of the samples, and it was collinear to the z direction of the reference frame used to define the dielectric function (see Fig. 2). Accordingly, the crystallographic axis c, coincided with the y direction of the same reference frame and laid on the sample surface. The crystallographic axis a, also laid on the sample surface and made an angle of 28.43° respect to the x-axis of the reference frame.

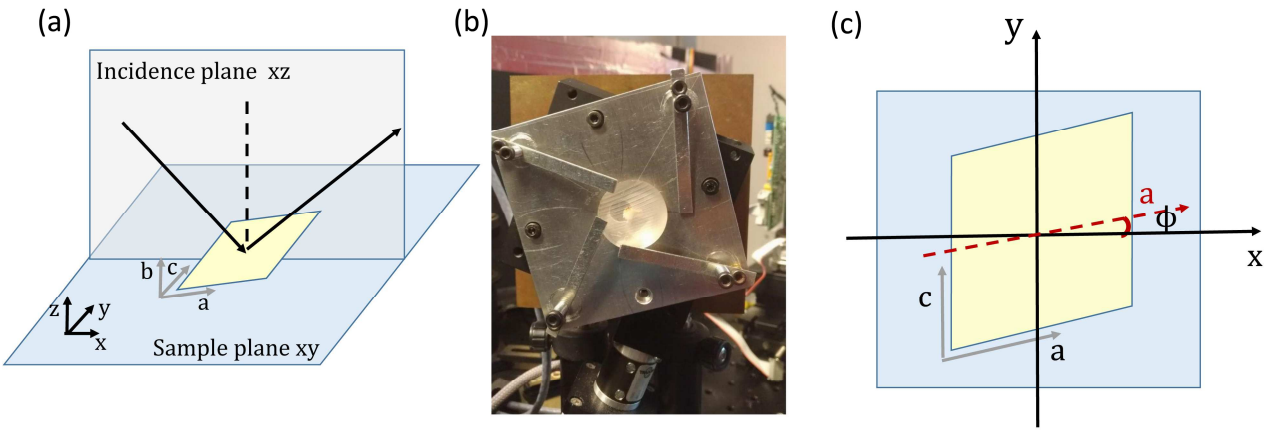

Fig. 2 – (a) Scheme of the measurements geometry showing the crystal orientation respect to the sample plane xy and the incidence plane xz; (b) Picture showing the sample position configuration in the ellipsometer used in this work; (c) Schematic representation of the crystal orientation in the xy sample plane, showing the azimuthal angle ϕ of the crystal (c axis) with respect to the plane of incidence (x axis).

In order to be measured with the infrared Mueller ellipsometer (Fig. 3), the samples had to be embedded in epoxy resin and polished down to 1 micron (RMS). It was also necessary to cut and handle the sample so that the samples' top and bottom surface were parallel to each other and keeping attention to the crystallography of the samples (cutting them along the crystal plane of the mineral is the perfect solution for performing such kind of measurements).

The final sample preparation procedure was defined as follows:

- Step 1 –the bulk materials are cut in smaller pieces (with dimensions of ~1 cm width and ~ 1-2 mm of thickness, compatible with the sample-holder used in the infrared Mueller ellipsometer) keeping attention to the parallelism of the two surfaces of the sample;
- Step 2 –The cut fragments are embedded in epoxy (resin (90%) + hardener (10%)) and left in an oven at 42°C for ~three hours; exposure to such conditions allow the mixture epoxy + hardener to dry and at the same time will not trigger a phase change from gypsum to bassanite (Bishop et al., 2014).
- Step 3 –An hydraulic press is used to take out the sample from the sample holder;
- Step 4 –Polishing of the samples is performed as followed: - 1) pad used P320 – lubricant water – time: 20 s; 2) pad used P800 – lubricant water – time: 20 s; 3) pad used P1200 – lubricant water – time: 20 s; 4) pad used 3 um – lubricant diamond paste – time: 5 m; 5) pad used 1 um – lubricant diamond paste – time: 5 m; 6) pad used ¼ um – lubricant diamond paste – time: 10 m.

- Step 5 –After polishing, each sample is cut (keeping once again attention to the parallelism of the two surfaces of the polymer) to obtain a thickness of about 6 - 7 mm that is adapted to the sample holder of the instrument. This step can be avoided or modified depending on the sample holder.

2.2 Experimental setup

The experimental setup used for the optical measurements consists of an in-house broadband infrared Mueller ellipsometer designed to work in the mid-infrared range, from 5000 to 750 cm^{-1} (2 - 13 µm) (Garcia-Caurel et al., 2015). Measurements can be performed either in reflection or in transmission; for this work, we have chosen to use the reflection configuration because it is the most sensitive configuration to measure isotropic and anisotropic substrates. The infrared Mueller ellipsometer is installed at the SOLEIL Synchrotron laboratories (France) and is composed of a light source, an input arm, an exit arm and an acquisition system (Fig. 3). The illumination source is a commercial FTIR spectrometer providing an infrared beam in a continuous spectral range from 750 to 5000 cm-1 (2 - 3 µm) with an infrared elliptic spot size on the sample (because of the oblique angle of incidence) of 1.5 mm and 3 mm dimensions (small and big axis of the ellipse, respectively). The FTIR spectrometer is equipped with a mid-infrared global source, a KBr beam splitter and a liquid nitrogen cooled MCT detector. The input arm is a Polarization State Generator (PSG) composed by a fixed linear polarizer (wire-grid type) and an achromatic retarder mounted in a rotatable holder. In the PSG, a sequential rotation of the retarder respect to the transmission axis of the fixed polarizer allows generating a set of different polarization states. The exit arm of the Mueller Ellipsometer consists of a Polarization State Analyzer (PSA) with the same optical components of the PSG but mounted in reverse order. The PSA analyzes the polarization of the incoming beam using a set of analysis configurations. Each analysis configuration is set by orientating the retarder in the PSA respect to the axis of transmission of the polarizer in the PSA at a given angle. During normal operation, the PSG generates four different polarization states and the PSA analyzes each of these polarization states with four analysis configurations.

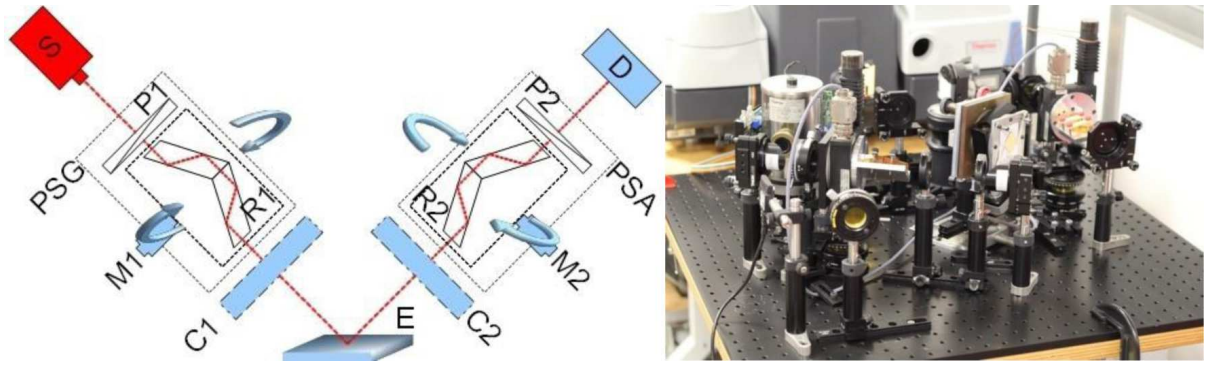

Fig. 3. Left: Schematic representation of a Mueller infrared ellipsometer. Right: picture of the Mueller infrared ellipsometer installed at the SOLEIL laboratories and used for the measurements performed in this project. P1 and P2 (linear polarizers), R1 and R2 (retarders), C1 and C2 (retractable calibration samples); E (sample); M1 and M2 (motorized rotation stges), S (IR source) and D (detector).

The result of an ellipsometric measurement is a set of sixteen independent values that allows calculating the Mueller matrix of the sample (Garcia-Caurel et al., 2015). This key matrix contains the information about the basic polarimetric effects on the beam light during the measurements. The Mueller matrix of an isotropic sample in reflection can be expressed in terms of the ellipsometric angles Δ and Ψ and is given by:

$$\mathbf{M}(\tau, \Psi, \Delta) = \tau \begin{pmatrix} 1 & -\cos(2\Psi) & 0 & 0 \\ -\cos(2\Psi) & 1 & 0 & 0 \\ 0 & 0 & \sin(2\Psi)\cos\Delta & -\sin(2\Psi)\sin\Delta \\ 0 & 0 & \sin(2\Psi)\sin\Delta & \sin(2\Psi)\cos\Delta \end{pmatrix} \quad \text{(eq. 1)}$$

where Δ and Ψ measure the change on the polarization state of a beam after reflection or transmission by a sample (Azzam and Bashara 1987). In particular Ψ is related to the change of intensity between the reflected component of the beam light with polarization parallel to the plane of incidence ('p') respect to the one with polarization perpendicular to the plane of incidence ('s'), while Δ measures the phase variation between these two components. For an isotropic sample, Δ and Ψ are in turn, related to the Fresnel reflection coefficients through the following relation:

$$\rho = \frac{r_p}{r_s} = \tan\Psi e^{i\Delta} \quad \text{(eq. 2)}$$

where r_p and r_s are the Fresnel reflection coefficient in polarization parallel and perpendicular to the plane of incidence, respectively. The relation reported above, is known as the fundamental equation of ellipsometry. From the measured parameters Δ and Ψ, the optical and structural properties of the

sample can be determined by appropriate modeling, as described in detail in Section 3 and Appendix A.

Ellipsometric measurements were acquired between 5000 and 750 cm^{-1} (2 and 13 μm) with a spectral resolution of 4 cm^{-1} (0.04 μm around 10 μm). In measuring the gypsum samples, several test measurements were performed with the aim of properly aligning the sample respect to the direction of the incident beam light. The number of test measurements done for each sample is not fixed and depends on the time required to find the ‘‘right’’ positions and it increases for anisotropic samples.

Once the sample was properly oriented, the integration time was increased to 32, 64 and even 128 integrations per polarization state, to reduce random noise and therefore to improve the signal to noise ratio.

The time required for the measurements increased a lot in the case of anisotropic samples because different azimuthal angles had to be taken into account, as discussed in Appendix A.

In parallel, reflectance measurements were performed with a FTIR Micro-spectrometer installed at SOLEIL to have a comparison standard for the ellipsometric measurements. The FTIR Microspectrometer is a Continuum microscope coupled to Thermo Nicolet 8700 FTIR spectrometer (Thermo Fisher). Samples were measured in the spectral range 6000 – 650 cm^{-1} (1.5 – 15 μm). Spectral resolution was 4 cm^{-1} (0.04 μm around 10 μm). Objective used was 15x (0.58 NA).

Thanks to the use of the micro-spectrometer, it has been possible to map the surface of the sample and to acquire spectra from different areas of the sample surface, in order to evaluate the presence of inclusions and to estimate their effect on the average spectra and on the ellipsometric measurements.

3. Data modeling

Ellipsometry is an indirect characterization technique, which means that to extract the optical constants from the measurements a model that allows their theoretical calculation has to be set up. An ellipsometric measurement evaluates polarimetric data (ellipsometer angles or Mueller matrices), but not the required parameters like thickness and optical constants. It is thus necessary to create a model of the sample to determine the sample parameters. Once the model is built, calculated data (Mueller matrix elements and retrieved optical constants) must be fitted to the experimental data and the best match between the two sets has to be found. The user has to evaluate the model that “best fits” the experimental data in order to decide if the model is physically reasonable and if the parameters resulting from the fitting routine are valid. Once the best fit is

obtained, the given model is considered the most sensible representation of reality. Thus, the values for the modeling parameters (like the optical constants) will be considered as the ones representing the real values.

Different options may be chosen in the selection of an appropriate model for the description of the spectral dependence of the optical constants of the material(s) under examination. The choice depends, primarily, on the material(s) and also on the spectral range selected for the analysis (Jellison G.E. 1993). In the infrared spectral range, a constant refractive index (ε_∞) is usually used to represent the contributions of the dielectric function at frequencies higher than the infrared. For each spectral feature present in the experimental data related to a vibrational mode a Kim oscillator is added. This type of oscillator is an extension of the simple harmonic oscillator model for vibrational modes (Kim et al., 1992). The Kim oscillator allows a continuous shift of the line shape between a Gaussian and a Lorentzian profile and is given by the following relations:

$$\varepsilon(\omega) = \varepsilon_\infty + \frac{A}{\omega_0^2 - \omega^2 - i\,\omega\,\Gamma(\omega)}$$

$$\Gamma(\omega) = \Gamma_0 \exp\left(-\left(\frac{1}{1+\sigma^2} \right) \left(\frac{\omega - \omega_0}{\Gamma_0} \right)^2 \right) \qquad \text{(eq. 3)}$$

where A is the intensity of the oscillator, ω is the position, Γ is the amplitude and σ is called Gauss-Lorentz-switch. Like almost all fitting parameters, σ may vary between 0 and infinity. For σ = 0 a Gaussian line shape is achieved, while large values of σ (larger than 5) lead to a Lorentzian. This latter feature is very advantageous because it allows to properly represent line shapes of multiple materials in either solid (crystal or amorphous) or liquid phase.

The use of the Kim oscillator is convenient, because it also requires a much less computational effort respect to other oscillators, like for example the Brendel oscillator (Brendel, 1990). This means that, working with many Kim oscillators and combining them, allows to save computational time and effort.

The optical response of real anisotropic samples can be very complex because of the presence of multiple resonance peaks whose position and intensity may vary as a function of the orientation of the sample respect to the direction of propagation of the light. Each resonance peak is linked to a particular vibration mode of the chemical bonds present in the crystal. In a crystal, each bond has a well-defined orientation in space and therefore reacts in a proper way to polarized light. Dielectric tensors are commonly introduced in optical models to represent the rich and complex optical response of anisotropic media. A general dielectric tensor has six independent elements, but if this

can be diagonalized, then, only three independent elements must be considered. The diagonalized dielectric tensor can be used to represent for instance orthorhombic, tetragonal or rhombohedral crystals; however, triclinic and monoclinic crystals (such gypsum) are characterized by non-diagonalizable dielectric tensors with more than three independent components. In the present study, however, for reasons related with compatibility with the software used to model and treat data, a diagonal tensor has been used. Therefore the crystal has been treated as orthorhombic, which is an approximation. The validity of this approximation is discussed in the following sections of the manuscript when we compare our results with data available in the literature (Section 5).

Although even the simplest parametric function used for each tensor component includes a number of oscillators and a constant term, difficulties may arise when it comes to assign the resonance peaks observed in the experimental data to the correct tensor components. This assignment is not obvious, and the difficulty increases with the number of resonances observed in the data. In order to deal with such an intricate situation we profited from the fact that the dichroism created by an infrared active vibration is maximal (minimal) when the polarization of the incident beam is parallel (perpendicular) to the chemical bond at the origin of the vibration. Therefore, we measured the sample at different azimuthal angles for which the amplitude of the observed absorptions reached either maxima or minima. In a second step, we assigned each one of the observed absorptions to Kim oscillators in the tensor component oriented along with the direction for which the amplitude of the absorption was observed to be maximal.

More details about the use of spectral features in the different Mueller matrix elements to assign vibrations to a given tensor component is provided in Appendix A with the description of two case studies.

The sample in the optical model used for this work is assumed to be a semi-infinite slab made of a homogenous material. The semi-infinite media implies that the only optical signal that is considered to the analysis is generated by light reflected by the uppermost surface (front face) of the sample. The influence of light coming from the back face of the sample, and therefore interference effects among light reflected by front and back face is not considered. This hypothesis, which is quite simplistic, is compatible with the type of samples considered in this study because they only had a single face polished to an optical level. Light reaching the back face of the samples, which was intentionally left unpolished, was scattered and not collected by ellipsometer.

The pseudo-dielectric function $\langle\varepsilon\rangle$ is used together with the elements of the Mueller matrix to represent the optical response of the sample. The pseudo-dielectric function depends on the elllipsometric angles Ψ and Δ and the angle of incidence, θ_0, according to the following expression:

$$\langle \varepsilon \rangle = \sin(\theta_0)\left[1+\left(\frac{1-\rho}{1+\rho}\right)^2 \tan^2(\theta_0)\right] \quad \text{with} \quad \rho = \tan(\psi)\exp(i\Delta) \qquad \text{(eq. 4)}.$$

When (eq. 4) is applied to the polarimetric data retrieved from an isotropic and semi-infinite sample, the pseudo-dielectric function represents the true dielectric function of it. This observation implies that the optical constants, refractive index and absorption coefficient of the sample, can be obtained without any model, which is a clear advantage in particular when considering remote sensing approaches in an astrophysical context. When, instead, the same equation is applied to an anisotropic sample, it provides the equivalent dielectric function of an isotropic material that would produce the same ellipsometric angles than the anisotropic material (Azzam and Bashara 1987). The pseudo-dielectric function of an isotropic material does not depend on either the angle of incidence or the azimuthal angle of illumination, even though in general, the effective dielectric function of an anisotropic material depends on both these angles. This property of the pseudo-dielectric function can be used to discern between isotropic and anisotropic materials, and in some cases, allows one to identify the type of anisotropy of the considered material, reason why we include this observable in our analysis. Moreover, the value of the pseudo-dielectric function can provide an approximate value of the mean dielectric function (i.e. an average of the components of the dielectric tensor). This information can be used as a guide to select reasonable values as guess to launch the data-fitting algorithms. It is important to recall here that, in general, the pseudo-dielectric function of an anisotropic material does not correspond exactly to the mean dielectric function of the same. Therefore, the pseudo-dielectric function should be used with the purposes above described, and, never to be interpreted as the mean dielectric function, that is instead being used to model the response of polycrystalline materials with randomly oriented anisotropic crystallites, commonly found in terrestrial and extraterrestrial soils, rocks or even meteorites.

Although in Appendix A, we show the interest of using multiple angles of incidence and multiple azimuths to orient the construction of the theoretical dielectric tensor model, in the present study, due to the type of samples used, it was not possible to modify the angle of incidence of the Mueller infrared ellipsometer, reason why only measurements done at a fixed angle of incidence and different azimuthal orientations were used. In order to simultaneously take into account the information provided by measurements at different azimuths, a multi-model capable of handling multiple data sets was used to simulate spectral Mueller matrices and to fit them to the corresponding experimental measurements. The best fitted parameters allowed the extraction of the optical constants of the material.

4. Results

An illustrative example of some of the data obtained from the gypsum samples measured is shown in Fig. 4 together with the best fitted simulations retrieved from the optical model.

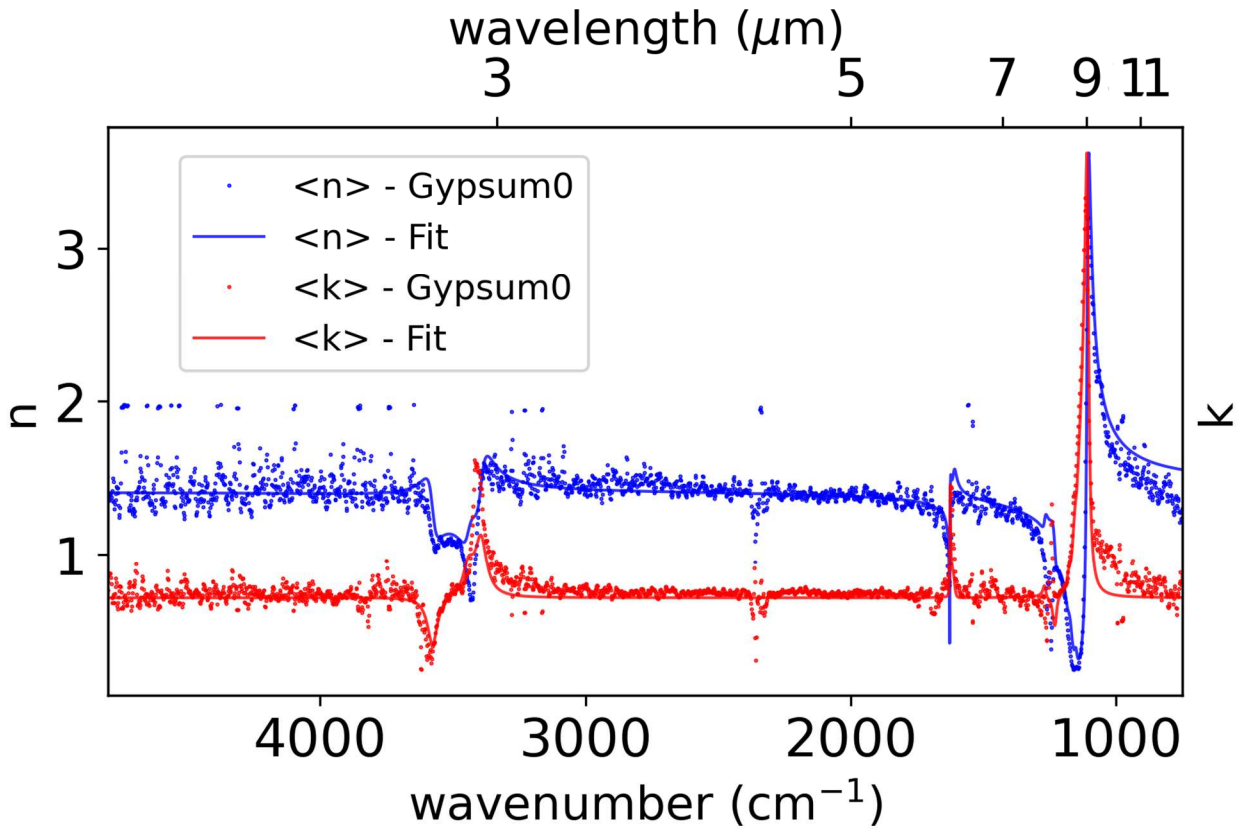

Fig. 4. Experimental and best-fitted theoretical data obtained for the gypsum sample. The results showed correspond to the pseudo refractive index (<n>) and pseudo absorption coefficient (<k>) of the sample oriented at an azimuth of 0° respect to the plane of incidence. A negative pseudo absorption coefficient is related to a vibration out of plane (z direction) as discussed in the text.

After modeling the gypsum data, it was possible to obtain a complete characterization of the optical constants for the three tensor's components ε_x, ε_y and ε_z. The corresponding values, in the n, k representation, are shown in Fig. 5.

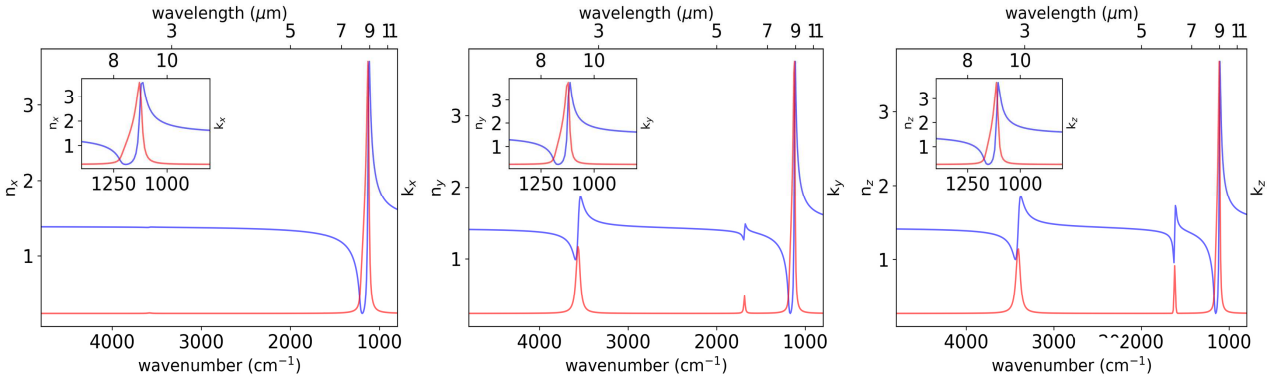

Fig. 5. Optical constants obtained for the gypsum sample (M14) along the three different components of the dielectric tensor, x, y and z obtained in this work. Inset plots (zoom on the spectral feature around 1100cm^{-1}).

In addition to the ellipsometric measurements, an FTIR micro-spectrometer was used to map the sample surface and to obtain a series of different non-polarized reflectance spectra which created a sort of spectral microcartography of the gypsum sample. In this way, it was possible to evaluate the effect of inclusions and roughness in the optical response of the samples used in this work. Representative examples of these measurements are shown in Fig. 6 in which it is possible to see a microphotography taken at low magnification (Fig. 6a) in the visible spectral range, taken with an auxiliary camera installed in the micro-spectrometer. In the selected area it is possible to see the surface of gypsum in light gray and one inclusion in dark gray. The three other images (Fig. 4b-d) correspond to three areas in Fig. 6a imaged with higher magnification. Area 1 and Area 3 show very similar spectra, which indeed overlap and shown in Fig. 6 (bottom panel). Those regions can be considered as representative of the majority of the sample surface. The spectrum of Area 2 show a peak located at 1150 cm^{-1} (8.6 µm) much less intense than the peak of gypsum at 1100 cm^{-1} related to sulfate ion absorption present in Area 1 and Area 3. As can be seen in the image of Area 2, the inclusions show a rougher surface than that of Area 1 and Area 3, therefore the scattering level may be much more important, which explains why the signal level from regions similar to Area 2 is less intense. Considering that the signal level coming from inclusions is less intense than that of gypsum and that the portion of the sample covered by inclusions was marginal (around 5% considering the whole sample surface) compared to that of gypsum explain why the eventual inclusions present in the sample did not show a noticeable effect neither in the ellipsometric measurements or the optical constants of gypsum derived from them.

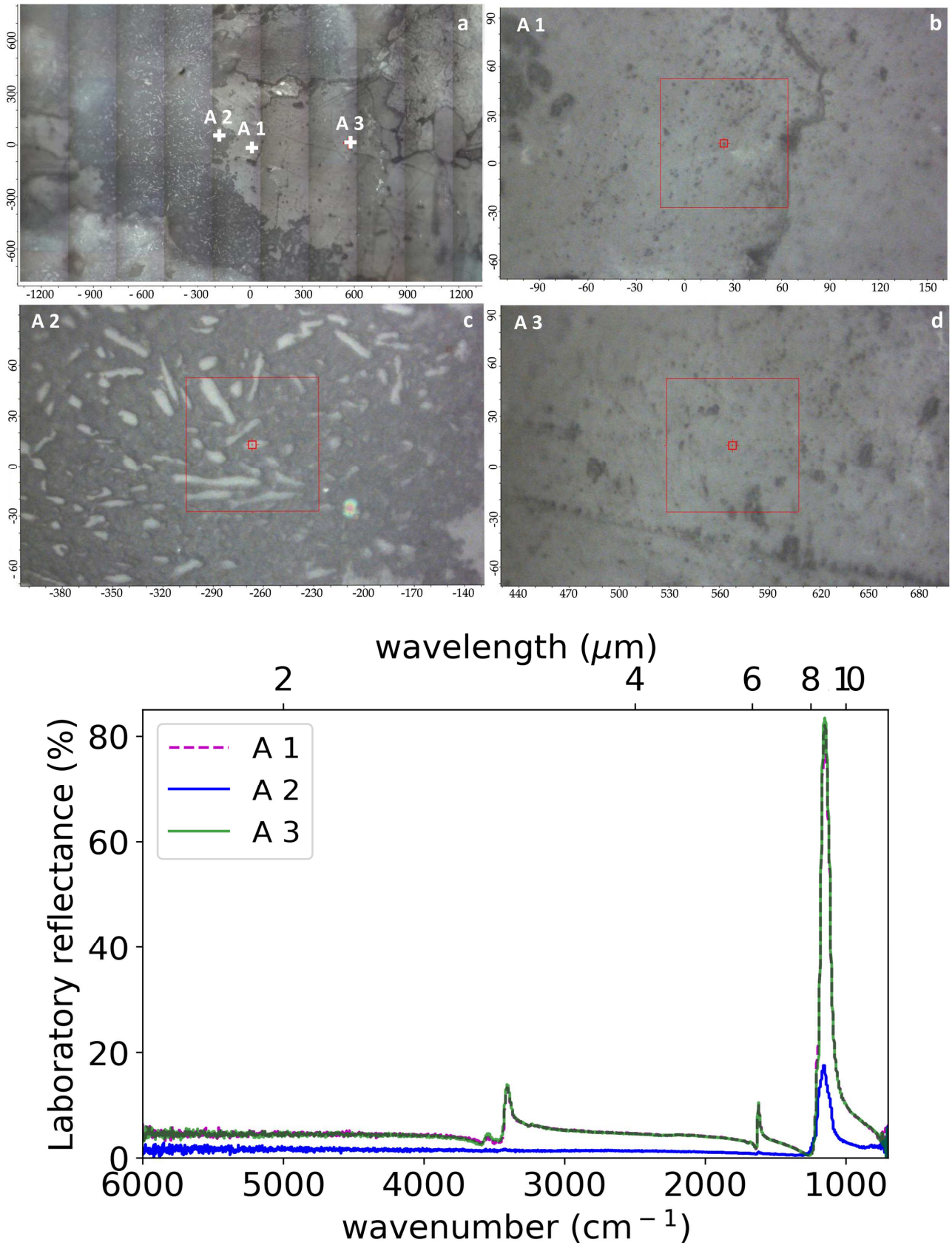

Fig. 6 – Upper panels - a) microphotography taken at low magnification of the surface of the sample M14 analyzed at the FTIR MicroSpectrometer; three white crosses indicates Area 1, Area 2 and Area 3 (A1, A2,

A3), where the spectra were acquired. b) zoom of Area 1; c) zoom of Area 2; d) zoom of Area 3; Bottom panel - spectra acquired from the three different areas of the sample surface.

5. Discussion

While performing our experiments, we observed that both sample preparation and data modeling must be done carefully. The sample preparation procedure described in section 2 has been refined after several tests. It has been observed that for raw minerals with non-polished surfaces, light was highly scattered, therefore almost no light reached the detector because the aperture of the instrument is quite small (just a tenth of a degree). For double-polished samples, back face contributions give non-coherent reflections, which are very difficult to take into account when it comes to building a parametric dielectric tensor. The back face of the sample much hence remain unpolished. Finally, for samples prepared as thin sections and embedded in epoxy resin, some loss of signal has been observed when the polishing protocol results in polished, but not planar surfaces. Samples prepared in thin sections are a good solution thanks to the fact that in most cases, the back portion of the sample that is embedded in the polymer is neither flat nor polished and therefore scatters light away from the specular direction, which avoids the reflection from the back surface. Despite of the net advantage, two problems were still present: i) the samples, although being polished one face, scattered a large amount of the light which reduced the signal level and increased the noise in the final data; ii) the two faces of the polymer holder in which the samples were embedded, were non-parallel, the latter was a problem when the azimuth was changed because the beam wandered and went out of the detector easily. In such cases, it was necessary to carefully tilt the sample-holder to realign the beam while trying not to change the angle of incidence.

In Fig. 7 we show a comparison of the optical constants (n and k) retrieved from this work with data found in the literature for gypsum, in particular for the values given by Long *et al*. (1993) and Roush et al. (2007). Long *et al*. (1993) measured two crystalline samples of gypsum cut such that one plane was parallel to two axes forming the monoclinic plane and the other was parallel to the third axis, allowing data to be acquired with the electric field parallel to each axis. Those data were treated in the framework of the dispersive analysis theory to obtain the dispersion of the different components of the dielectric tensor. The results discussed by Roush *et al.* (2007) were obtained combining diffuse reflection and transmission data measured on grain fractions of samples after applying different corrections based on scattering theories. From the several results discussed in Roush *et al*. (2007), the ones shown in Fig. 7 correspond to those derived from diffuse reflectance only for consistency with results in Long *et al*. (1993) and in the present work.

As it can be seen in the results shown in Fig. 7, the three studies agree with the fact that the optical response of gypsum in the measured infrared spectral range is dominated by three non-overlapping spectral features situated at around 1100 cm^{-1}, 1629 cm^{-1} and 3500 cm^{-1}. The assignment of these features to particular vibration modes is well known in the literature (for more details see Bishop et al., 2014; Seidl et al., 1968; Haas & Sutherland 1956). The feature at 1150 cm^{-1} is attributed to the stretching vibrations of the O-S-O bonds in the sulphate units in the gypsum crystal. The unit cell of gypsum includes different sulphate tetrahedra which are oriented along different directions in space, reason why the spectral feature corresponding to the O-S-O stretching has an influence on the three components of the dielectric tensor. Water molecules are preferentially oriented parallel to a plane which contains the crystallographic axes *b* and *c* (e.g. Haas, 1956; Seidl, 1968). For this reason, the spectral features around 1629 cm^{-1} and 3500 cm^{-1} related to water vibrations show contributions to the ε_y and the ε_z components of the dielectric tensor only.

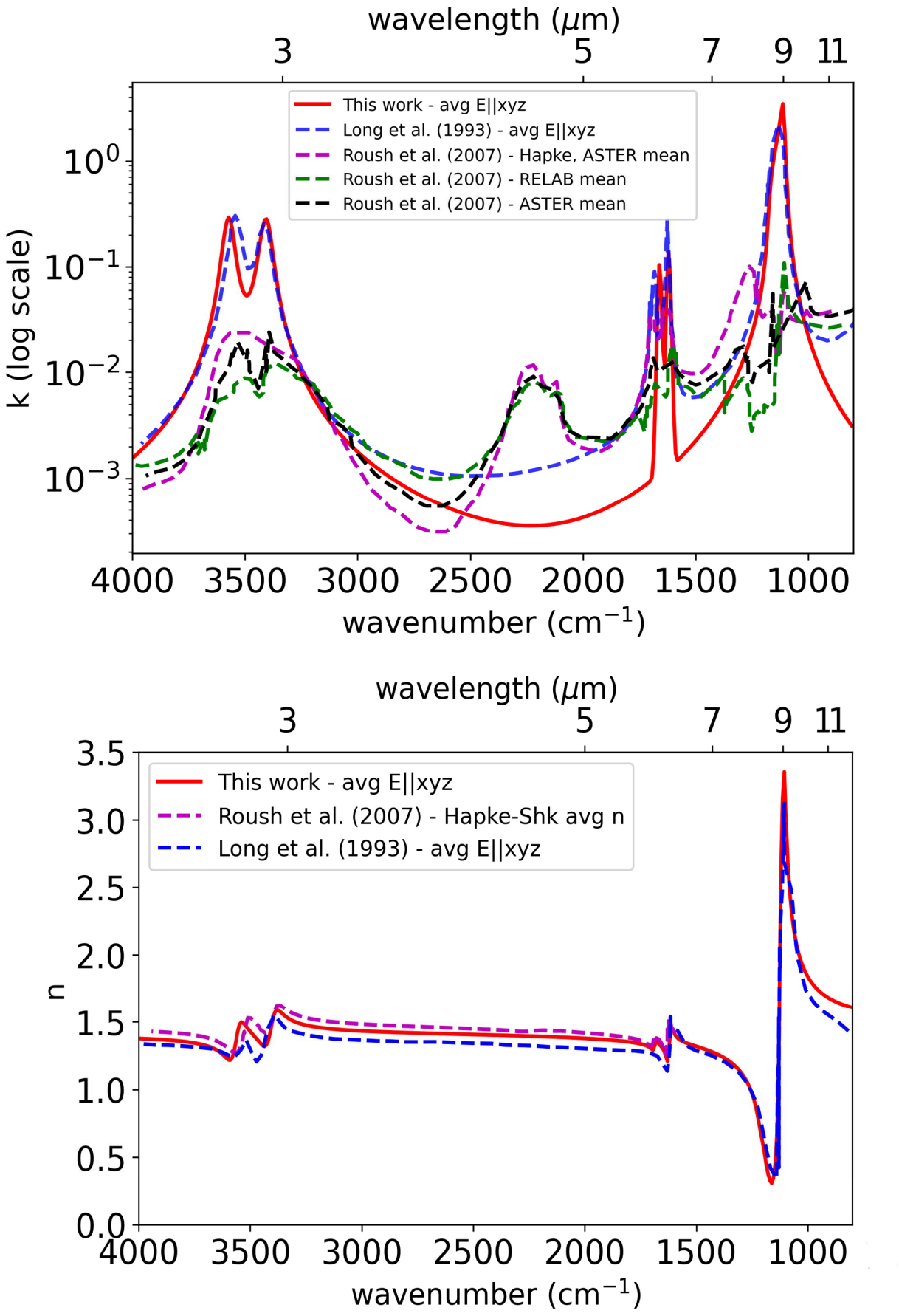

Fig. 7. Comparison between k (upper panel) and n (bottom panel) obtained in this work and in the work of

Long et al. (1993) and Roush et al. (2007).

Despite of the above mentioned agreement, there are also some discrepancies between the set of results shown in Fig. 7. The most relevant difference is the broad absorption peak around 2300 cm^{-1}, which can be attributed to overtone ($2v_3$) of the v_3 main vibration of the SO_4 group (Fink and Burk, 1973). This absorption peak is present in the results from Roush *et al.* (2007), and absent in both, the results discussed by Long *et al*. (1993) and the ones in the present work. Absorptions due to band combinations are in general weak, and they are more easily observed in transmission than in reflection measurements. The fact that the experimental data discussed in Roush *et al.* (2007) are partially based on transmission measurements, may explain why they were able to detect the absorption centered around 2300 cm^{-1}.

A second discrepancy between the results from Roush *et al.* (2007) and both, the results from Long *et al.* (1993) and the ones presented in the present work, are the intensity and the overall shape of the absorption peaks around 3500 cm^{-1} and 1100 cm^{-1}. In general, the absorption of the two peaks around 3500 cm^{-1} and 1100 cm^{-1} appear to be one order of magnitude larger in the work of Long *et al*. (1993) and the present work compared to the estimation provided by Roush *et al.* (2007). The origin of these discrepancies may be explained because Long *et al*. (1993) and the present data were obtained from measurements performed in polished samples, while the results discussed in Roush *et al*. (2007) were obtained from grain fractions of samples after being corrected using different scattering theories. As Roush *et al*. (2007) mentioned in their work, scattering theories perform well for transparent and weakly absorbing spectral regions, while they produce results with high uncertainty in spectral regions characterized by strong absorption. To estimate strong absorption coefficients, Roush *et al*. (2007) recommend to use reflection data (either specular or diffuse). Since the peaks at 3500 cm^{-1} and 1100 cm^{-1} correspond to strong absorptions, it seems probable that results based on scattering theory underestimate to some extent the actual value of such absorptions.

The intensity of the band at 1629 cm^{-1} show comparable values according to Long *et al*. (1993), the present work and the Hapke scattering model from ASTER data discussed in Roush *et al*. (2007). According to the results from Roush *et al*. (2007), shown in Fig. 7, the estimated value of the absorption band at 1629 cm^{-1}, considerably depends on the scattering theory used to correct the raw data. However, and according to Roush *et al.* (2007), since the absorption coefficient obtained from transmission measurements (see fig. 14 in Roush *et al*., 2007) coincide with the estimation using the Hapke model, it seems plausible that the Hapke approximation provides a good estimate for the actual absorption in this spectral region. Moreover, since the absorption coefficient obtained with the Hapke approximation is comparable with the values by Long *et al*. (1993) and the present work,

the authors think that the three of them are consistent to each other, and are good estimates of the absorption coefficient around 1629 cm^{-1}. The question why the Hapke model works well at 1629 cm^{-1} but fails to provide good results for the peaks at 1100 cm^{-1} and 3500 cm^{-1} is mentioned by Roush *et al*. (2007) although a definitive answer is not provided.

Besides the measurement configuration (reflection, transmission) and the approach used to correct the raw experimental data, different factors such hydration level, concentration of impurities, the origin and the history of the mineral used as a sample, can also play a role to partially explain some of the differences observed between data obtained from different samples at different times. Regarding the present work, since the authors did not had access to the original samples discussed by Long *et al*. (1993) and to Roush *et al*. (2007) it was not possible to estimate to which extent the above mentioned factors can be responsible of the variations between data shown in Fig. 7. Although a systematic study can reveal the exact contribution of each of those factors to the finally extracted value of the absorption coefficient, it seems plausible regarding the data in Fig. 7, that their effect is marginal compared to that of method used to measure and to treat the data.

On the basis of the above discussion, we agree with Roush *et al*. (2007) that measurements in reflection are very sensitive to determine the value of strong absorption coefficients, such the ones of the peaks at 1100 cm^{-1}, 1629 cm^{-1} and 3500 cm^{-1}, but when it comes to determine the absorption coefficient of weak absorptions, the use of data in transmission or a combination of reflection and transmission measurements, when it is possible, may provide the most sensitive data and reliable results. At this point, we would like to recall that data in reflection configuration is the most likely to be obtained from orbiters or a probes landed on Mars surface.

In summary, it can be said that the ellipsometric method based on measurements in reflection configuration presented in this work is an appropriate method for the determination of the dispersion of the three components of the dielectric tensor due to the main absorption peaks that characterize the measured sample. Moreover, the overall agreement between the optical constants obtained in this work and those discussed in the literature validates the ellipsometric method, and the data treatment protocol discussed in this work.

6. Summary and Conclusions

In this work, an experimental approach based on spectroscopic Mueller ellipsometric measurements has been used on gypsum samples as an example of the validity of this technique for the determination of optical constants of planetary analog samples. Although ellipsometric measurements for materials characterization are common in materials science and the

semiconductor domains, this is the first time that the method is proposed to characterize planetary analog samples for the astronomical community. Keeping the latter in mind, in this paper we illustrate with a simple model the optical response of an anisotropic material when it is studied with an ellipsometric approach. To this end, we show the interest of performing, when possible, measurements at different angles of incidence and azimuths, in order to highlight the contribution of each one of the components of the dielectric tensor of the sample under study. Moreover, we illustrate the use of the information that could be retrieved from measurements to build an optical model of the dielectric tensor, which in turn has to be used to model the experimental data. Working with real minerals required a careful study of the sample preparation method in order to get samples in a way that could be analyzed with the ellipsometric approach. Not properly prepared samples can cause time-consuming measurements, difficulties in sample alignment and, quite complex data modeling for anisotropic samples.

The main goal of this work is to develop a new laboratory approach for the experimental determination of optical constants of minerals of planetary interest. These data, scarce in literature, are crucial for the correct interpretation of spectral data from planetary surfaces. In the case of Mars, knowledge of optical constants is essential in the framework of spectral modeling, to invert and deconvolve spectra of its surface and aerosols.

The optical constants of gypsum obtained in this study in the MIR spectral region using the spectro ellipsometric method compare well with data obtained by other authors, which validates the approach. It is important to remind here that the optical model used in this study is an approximation for monoclinic and triclinic crystalline materials. Since a vast majority of clay materials and other analogs of Mars surface are either triclinic or monoclinic, in the near future, a more accurate model, including non-diagonalizable tensors, and based in the dispersion theory approach is going to be used to improve the accuracy of the results obtained with this ellipsometric technique.

In this perspective, a near future goal will be to optimize the measurement protocol, for instance, to prepare the sample in a way in that it will possible to know in advance the crystal orientation. Moreover, the technical configuration of the ellipsometer will also be improved to be able to perform measurements at multiple angles of incidence and at multiple azimuths to get the most from the samples as discussed in this paper and in Appendix A. All the above optimizations will surely allow the extension of the experiments to a wide range of planetary analogues and other materials of astrophysical interest.

Acknowledgements

This project was founded by NASA-JPL under grant agreement n° KM-2691-947266. R.G.U. thanks the CNES postdoctoral program.

References

Alemanno G., Orofino V. & Mancarella F.: 2018, Global Map of Martian Fluvial Systems: Age and Total Eroded Volume Estimations. Earth and Space Science 5, 560-577, doi: 10.1029/2018EA000362.

Anthony J.W., Bideaux R. A., Bladh K. W., Nichols M. C.: 1990, in Handbook of Mineralogy, Mineral Data Publishing, Tucson Arizona, USA, p. gypsum.

Arteaga O.: 2014, Useful Mueller matrix symmetries for ellipsometry, Thin Solid Films, Vol. 571, pp. 584-588.

Azzam R.M.A., Bashara N.M.: 1987 Ellipsometry and Polarized Light (Elsevier, Amsterdam).

Bibring J.P. et al.: 2006, Global Mineralogical and Aqueous Mars History Derived from OMEGA/Mars Express Data, Science, 312, 400.

Bishop J.L., Lane M.D., Darby Dyar M., King S.J., Brown A. J., Swayze G. A: 2014, "Spectral properties of Ca-sulfates: Gypsum, bassanite, and anhydrite", American Mineralogist, Vol. 99 p.p. 2105-2115.

Brendel R.: 1990, An infrared dielectric function model for amorphous solids, Journal of Applied Physics, 71, 587.

Carter J. et al: 2013. Hydrous minerals on Mars as seen by the CRISM and OMEGA imaging spectrometers: Updated global view. Jou. Geophys. Res. 118, 831-858.

Christensen et al.: 2001, The Mars Global Surveyor Thermal Emission Spectrometer experiment: Investigation description and surface science results, J. Geophys. Res., 106, 23,823-871.

Ehlmann B.L. and Edwards S.E.: 2014, Mineralogy of the Martian Surface, Ann. Rev. Earth Planet. Sci., 42, 291.

Fink U. and Burk S.D.: 1973, Reflection spectra, 2.5 – 7 μm of some solids of planetary interest. . Comm. Lunar Planet. Lab. 10, 8-20.

Formisano et al.: 2005, The Planetary Fourier Spectrometer (PFS) onboard the European Mars Express mission, Planet. and Space Sci., 53, 963 – 974.

Garcia-Caurel E. et al.: 2015, A mid-infrared Mueller ellipsometer with pseudo-achromatic optical elements, Applied Optics, 54, 2776-2785.

Jellison G.E.: 1993, Data analysis for spectroscopic ellipsometry, Thin solid films, Vol. 234, pp. 416-422.

Kim C.C., Garland J.W., Abad H., Raccah P.M.: 1992, Modeling the optical dielectric function of semiconductors: Extension of the critical-point parabolic-band approximation, Phys. Rev. B 45, 11749-11767.

Korablev et al.: 2018, The Atmospheric Chemistry Suite (ACS) of Three Spectrometers for the ExoMars 2016 Trace Gas Orbiter. Space Science Review. 214:7

Long L.L. et al.: 1993, Optical properties of calcite and gypsum in crystalline and powdered form in the infrared and far-infrared, Infrared Physics, 34, 191-201.

Marzo G.A. et al.: 2004, The optical constants of gypsum particles as analog of Martian sulfates, Advances in Space Research, 33, 2246-2251.

Murchie S. L. et al.: 2007, Compact Reconnaissance Imaging Spectrometer for Mars (CRISM) on Mars Reconnaissance Orbiter (MRO), Jou. Geophys. Res., 112, doi:10.1029/2006JE002682.

Orofino V., Alemanno G., Di Achille G., Mancarella F.: 2018, Estimate of the water flow duration in large Martian fluvial systems. Planetary and Space Science, 163, 83-86.

Pedersen B.F.: 1982, Neutron Diffraction Refinement of the Structure of Gypsum, CaSO4·2H2O, Acta Crystalographica, Vol. B38, pp. 1074-1077.

Poulet F. et al.: 2002, Comparison between the Shkuratov and Hapke Scattering Theories for Solid Planetary Surfaces: Application to the Surface Composition of Two Centaurs Icarus, Icarus, 160, 313-324.

Poulet, F., Erard, S., 2004. Nonlinear spectral mixing: Quantitative analysis of laboratory mineral mixtures. J. Geophys. Res. 109, doi: 10.1029/2003JE002179.

Poulet F. et al.: 2005, Phyllosilicates on Mars and implications for early Martian climate. Nature 438, 623-627, doi :10.1038/nature04274.

Poulet, F. et al., 2008. Abundance of minerals in the phyllosilicate-rich units on Mars. Astron. Astrophys. 487, L41–L44.

Poulet F. et al.: 2014, Mineral abundances at the final four curiosity study sites and implications for their formation, Icarus, 231, 65-76.

Roush T. L., Esposito F., Rossman G. R. , Colangeli L.: 2007, Estimated optical constants of gypsum in the regions of weak absorptions: Application of scattering theories and comparisons to independent measurements. Jou. Geophys. Res. 112, E10003, doi:10.1029/2007JE002920.

Seidl V., Knop O., Falk M.: 1969, Infrared studies of water in crystalline hydrates: gypsum, $CaSO_4 \cdot 2H_2O$, Can. J. Chem. Vol. 47, pp. 1361-1368.

Shkuratov, Y., Starukhina, L., Hoffmann, H., Arnold, G., 1999. A model of spectral albedo of particulate surfaces: Implications for optical properties of the Moon. Icarus 137, 235–246.

Stack K.M., Milliken R.E.: 2015, Modeling near-infrared reflectance spectra of clay and sulfate mixtures and implications for Mars, Icarus, 250, 332-356.

Vandaele A. C. et al.: 2015, Science objectives and performances of NOMAD, a spectrometer suite for the ExoMars TGO mission. Planetary and Space Science, 119, 233-249

Appendix A

A.1 Optical response of an ideal anisotropic and semi-infinite slab: two cases of study

In this Appendix we discuss two cases of study to illustrate the properties of the Mueller matrix of an ideal anisotropic material when measured either under different azimuthal orientations respect to a given reference axis, and under different angles of incidence for fixed azimuthal angles. The purpose of such examples is to show first, how the infrared resonant absorptions determine the spectral features in the Mueller matrix elements, and second, how the dependence of such spectral features with either the angle of incidence or the azimuthal angle can be used to assign the absorptions to the different components of the dielectric tensor of the sample.

The data used for the two examples have been generated with the same optical model described in the main text, which represents a semi-infinite slab of a homogeneous anisotropic material. The optical model considers samples to be in an orthogonal (reference laboratory) coordinate system. In the frame of the coordinate system, the orientation of the probing beam respect to the sample is defined by both the angle of incidence (i.e. the angle between the incident beam and the normal to the surface of the sample) and the azimuthal angle (i.e. the angle between the optic axis of the sample and the plane of incidence). The plane of incidence contains the incident beam and its projection on the sample surface. The optical properties of the simulated material have been represented using a diagonalizable tensor with only three components and therefore, triclinic and monocline materials are treated using an orthorhombic approximation. For clarity, the dielectric tensor of the material considered for the examples has been extremely simplified; it contains a single oscillator per tensor component. Clearly, the tensor used for the two examples does not represent gypsum, but a hypothetic, albeit realistic, material.

Each oscillator used to represent a resonant absorption is modeled using the Kim oscillator approach (see for instance Fig. A.1). The Kim oscillator equation allows the modification of the strength, position, spectral width and line shape of each resonance. Typical values for these parameters in the samples analyzed in this study are: ε_∞: 2.3, A (strength): $7x10^{-4}$, ω_0 (spectral position): 0.15 eV (1210 cm^{-1}), Γ_0 (spectral width): 0.003 eV (25 cm^{-1}), σ (Sigma): 0.1. Out of the resonance, the refractive index of the materials explored in this work is between 1.4 and 1.6, which remains close to that of typical non-metallic minerals including gypsum and other evaporites. Fig. A.1 shows the dispersion of a Kim oscillator with the parameters above-detailed. As can be seen,

the oscillator describes a moderate to feeble absorption because the refractive index never goes below one, or, equivalently, the real part of the dielectric function is always positive.

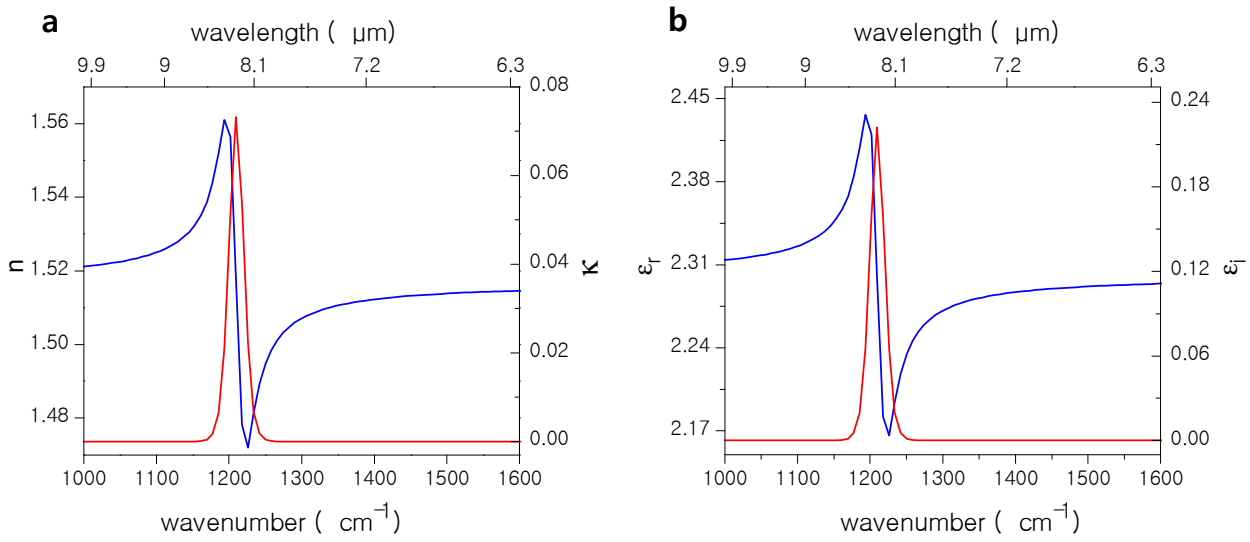

Fig. A.1 – (a) Dispersion of the values of the refractive index, *n*, and the absorption coefficient, κ obtained with an oscillator described in the text. (b) Same simulation, but using the real, ε_r and imaginary, ε_i, parts of the dielectric function as observables.

A.1.1 Anisotropic media: Influence of the angle of incidence

The case discussed here represents a very simple model of a biaxial material. A single oscillator is used for each one of the components of the dielectric tensor. The parameters used to build the dispersion of each component of the dielectric tensor are the following:

- ε_x : ε_∞=2.3, A=1x10^{-4}, ω_0=0.18 eV (1452 cm^{-1}, 6.88 μm), Γ_0=0.003eV (25 cm^{-1}, 0.23μm), σ=0.1.
- ε_y : ε_∞=2.3, A=1x10^{-4}, ω_0=0.16 eV (1290 cm^{-1}, 7.75 μm), Γ_0=0.003eV (25 cm^{-1}, 0.30 μm), σ=0.1.
- ε_z : ε_∞=2.3, A=1x10^{-4}, ω_0=0.14 eV (1129 cm^{-1}, 8.86 μm), Γ_0=0.003eV (25 cm^{-1}, 0.40 μm), σ=0.1.

To make things as simple as possible, the only difference among the parameters defining the oscillators is their respective spectral position. Moreover, the spectral position and width of the oscillators have been chosen to avoid any overlapping among them. In this way, the effect of each oscillator appears in a well-defined spectral region clearly identifiable, and therefore, it is possible to study how each of them influence the spectral dependence of the Mueller matrix. In an anisotropic material, both the angle of incidence and the azimuthal angle may in principle have an effect on the Mueller matrix of the sample. In our example we have chosen to vary first the angle of

incidence choosing three angles, one 10 degrees (46.6°) below the Brewster angle, θ_B, another one at θ_B (56.6°) and the third one 10 degrees (66.6°) above θ_B. These three angles have been chosen to show the interest of making measurements close to the Brewster angle, and also to illustrate the interest of studying the variation of the optical response with the angle of incidence to decide in which component of the dielectric function a given absorption should be. Fig. A.2 shows a selection of Mueller matrix elements, and the pseudo-dielectric function, for the three angles of incidence above mentioned. The Mueller matrix elements not shown in Fig. A.2 are either equal to a + or – sign to those shown, and therefore they do not carry any new information. For a full discussion about Mueller matrix symmetry in ellipsometry see for instance (Arteaga, 2014). In the three cases illustrated in Fig. A.2, the sample was oriented at an azimuth equal to 0° which in practice means that the ***x*** component of the dielectric tensor is parallel to the plane of incidence, the ***s*** direction, and correspondingly, the ***y*** component of the dielectric tensor is perpendicular to the plane of incidence, the ***p*** direction.

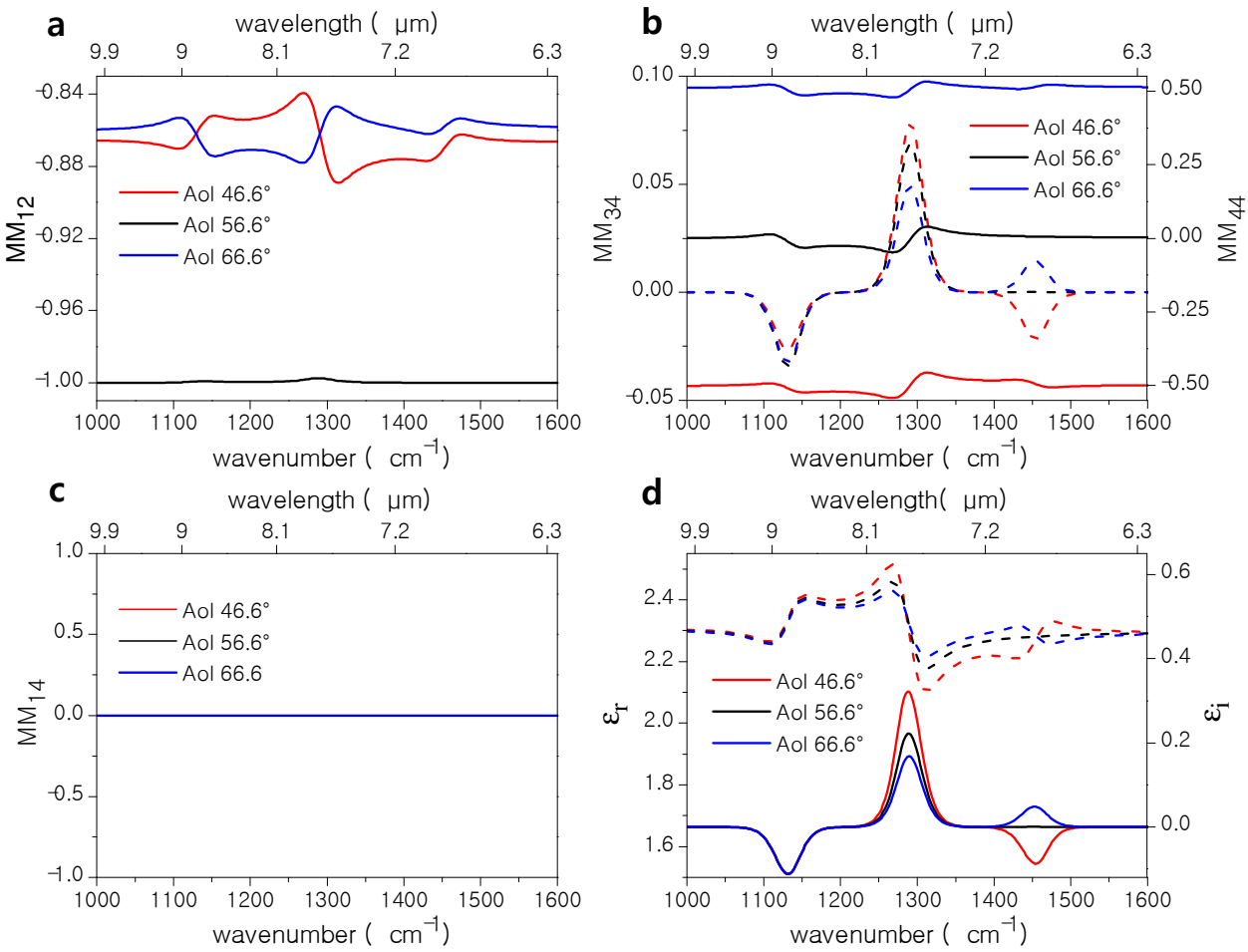

Fig. A.2 – a) Mueller matrix element M_{12} b) Mueller matrix elements M_{34} and M_{44} c) Mueller matrix element M_{14} d) Real, $\langle\varepsilon_r\rangle$, and imaginary, $\langle\varepsilon_i\rangle$, part of the pseudo-dielectric function. Dashed lines in b) and d) correspond to element M_{34} and $\langle\varepsilon_r\rangle$ respectively.

From the simulated data in Fig. A.2, it can be seen that the variation of the angle of incidence has an impact on all the elements of the Mueller matrix and the dielectric function as well. However, the variation is not the same for three components of the dielectric tensor. These differences can give indices for the identification of patterns in real data. In the Mueller matrix element M_{12}, the absorptions appear as inflections, some of them with positive concavity and the others with negative concavity. The absorption in the ε_z component has a positive concavity below θ_B and at θ_B, however it transforms to a negative concavity above θ_B. The absorption in the ε_y component, *s*-polarized, has a negative concavity below θ_B, and a positive concavity at θ_B and above it. The absorption in the ε_x component, *p*-polarized, is peculiar and illustrates the interest of measurements at θ_B or close of it; its concavity does not change with the angle of incidence, but disappears at θ_B. This property which is in accordance with the definition of θ_B in a dielectric material, is useful in practice because it allows the identification of the absorptions which are mainly *s*-polarized from the others, and therefore facilitates the assignment to the ε_x or ε_y component of the dielectric tensor provided that the azimuthal angle is known.

The Mueller matrix element M_{34} also gives interesting clues to assign absorptions to the corresponding component of the dielectric tensor. In the Mueller matrix element M_{34}, absorptions appear as peaks, whatever the angle of incidence; peaks are always negative for the ε_z component and positive for the *s*-polarized components (ε_y component in Fig. A.2). On the contrary, peaks for p-polarized components (ε_x component in Fig. A.2) are negative for incidence angles below θ_B, positive for angles above θ_B and null for at θ_B in accordance to the definition of Brewster angle.

The Mueller matrix element M_{44} shows information analogous to that of the matrix element M_{12} concerning peaks. The interest of this element is that for spectral regions out of resonance, it becomes negative for angles of incidence below θ_B, positive for angles of incidence above θ_B, and null at θ_B. The element M_{44} is therefore a good indicator to decide whether measurements are done at an angle of incidence close enough to θ_B.

Off-diagonal elements of the Mueller matrix such as M_{14} or M_{23} are null for azimuths 0° and 90°. The difference between absorption belonging to distinct components of the dielectric tensor is also well-visible in the dependence of the real and imaginary components of the pseudo-dielectric function with the angle of incidence. Absorptions in the component ε_z appear as negative peaks in

the $\langle\varepsilon_i\rangle$ and as inflections with positive concavity in $\langle\varepsilon_r\rangle$. Interestingly, either $\langle\varepsilon_i\rangle$ or $\langle\varepsilon_r\rangle$ does not show any variation with the angle of incidence for absorptions in the ε_z component, which is a very good clue to identify absorptions belonging to the out of plane component. Spectral features belonging to a *s*-polarized absorption (ε_y component in Fig. A.2) appear as an inflection with negative curvature in $\langle\varepsilon_r\rangle$ and positive peaks in $\langle\varepsilon_i\rangle$ the amplitude of the peaks or the inflections diminishes with an increasing angle of incidence, but there is no change of their respective sign.

Finally, for p-polarized absorptions (ε_x component in Fig. A.2) absorptions manifest as inflections with positive concavity below θ_B, negative concavity above θ_B, and they do not show any feature at θ_B. Correspondingly, the same absorptions appear as a negative peak for angles below θ_B, positive peaks for angles of incidence above θ_B, and they disappear at θ_B. The simulation shows that in the pseudo-dielectric representation each component of the dielectric tensor has a characteristic dependence, different to each other. For this reason, and despite of the fact that in general, the pseudo-dielectric function cannot be used to deduce with precision the value of the different components of the dielectric tensor, the use of this observable can help to properly assign oscillators to the different components of the dielectric tensor when it comes to build an optical model and to give an estimate of their respective strengths as well as for the average value of the constant ε_∞.

A.1.2 Anisotropic media: Influence of the azimuthal angle

The second parameter which can be scanned in a measurement run is the azimuth. In the following we show the effect of a rotation of the sample keeping an angle of incidence close to θ_B. The azimuthal angles chosen for the simulation are 0°, 45° and 90°. Simulations corresponding to azimuth 135° are not shown because they are redundant respect to simulations at an azimuth of 45°. In analogy to Fig. A.2, the data shown in Fig. A.3 correspond to a selection of Mueller matrix elements and the pseudo-dielectric function.

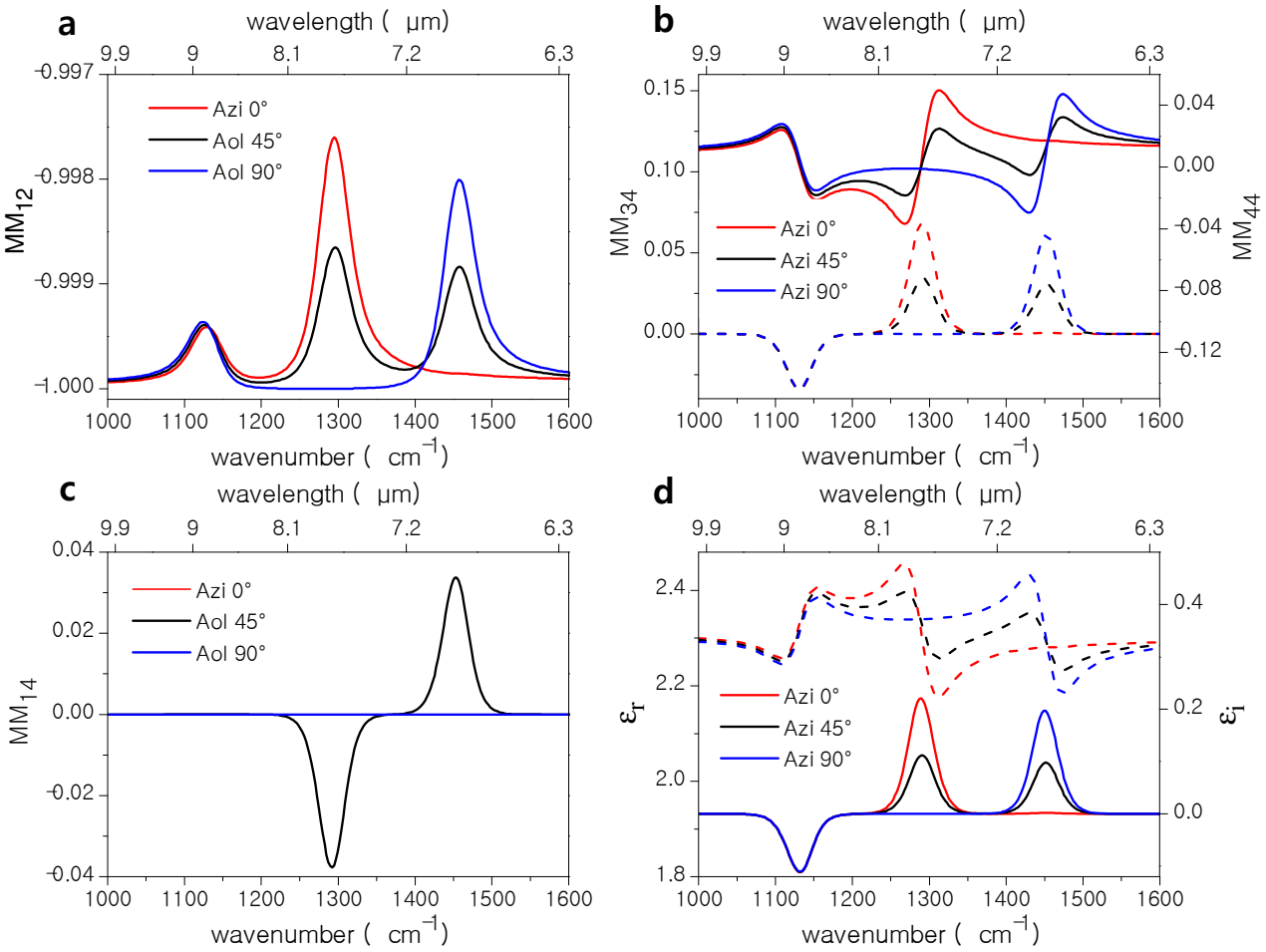

Fig. A.3 – a) Element M_{12} b) Elements M_{34} and M_{44} c) Element M_{14} d) Real $\langle\varepsilon_r\rangle$and imaginary $\langle\varepsilon_i\rangle$ part of the pseudo-dielectric function. Dashed lines in b) and d) correspond to element M_{34} and $\langle\varepsilon_r\rangle$ respectively.

Data for the azimuth 0° are the same shown in Fig. A.3, for an angle of incidence equal to θ_B. Mueller matrix element M_{12} shows that rotating the sample from azimuth 0° to 90° transforms the ε_y component of the dielectric tensor in *p*-polarized whereas the component ε_x becomes *s*-polarized. In consequence, the only peaks which are visible in the M_{12} at azimuth 90° correspond to the ones in the ε_z (out of plane) and ε_x (*s*-polarized), while at azimuth, 0° the visible peaks are those due to the ε_z and the ε_y components of the dielectric tensor. Since the features due to ε_z remain unchanged, a comparison of data at azimuths 90° and 0° is a good way to identify features to the ε_z component (the unchanged part), the features due to the ε_x component (disappear or get minimized at azimuth 0°) and the features due to the ε_y component (disappear or minimized at azimuth 90°). Mueller matrix element M_{14} is only sensitive to the in plane components, ε_x and ε_y, of the dielectric tensor.

Interestingly, the spectral features related to absorption appear as peaks. When the sample is turned to an azimuth of 45°, absorptions in the ε_y component appear as negative peaks while contributions

of the ε_x component appear as positive peaks. Rotating the sample to 135° (not shown in the figure for clarity) will change the sign of the peaks, but does not bring any new information respect to the orientation at 45°. Mueller matrix element M_{14} is thus very important to discriminate between contributions due to ε_x from those due to ε_y. The information that can be retrieved from the analysis of either the pair of elements M_{32} and M_{44}, or, the real and imaginary parts of the pseudo-dielectric function is quite similar. Contributions from the out of plane component, ε_z, of the dielectric tensor appear as a negative peak and an inflection with a positive concavity in $\langle\varepsilon_i\rangle$ and $\langle\varepsilon_r\rangle$ respectively. Contributions due to the out of plane component remain unchanged when the sample is rotated. Comparing measures taken at azimuth 0° and 90° allow to get information about the contribution of the in plane components ε_x and ε_y, because at 0° the contributions due to the ε_x component (*p*-polarized at azimuth = 0°) are minimized while at azimuth 90° the contribution of the ε_y component (*p*-polarized at azimuth = 90°) are in turn minimized.

The previous simulation shows the importance of taking data at different angles of incidence and azimuthal angles when characterizing anisotropic materials, to facilitate the task of building appropriate optical models.